2861

Comparison of Size and Morphology of Soot Aggregates As Determined by Light Scattering and Electron Microscope Analysis

J. Cai, N. Lu, and C. M. Sorensen*

Department of Physics, Kansas State University, Manhattan, Kansas 66506-2601

Soot particles were collected from premixed methane/oxygen flames using a thermophoretic sampling device. Transmission electron micrographs of the soot were optically scanned and stored digitally in a computer. These digitized images where analyzed to determine the mean soot cluster radius of gyration, fractal dimension, number of monomers per cluster, and monomer radius. Effects of three- to two-dimensional projection of the clusters during microphotography were evaluated. These morphological parameters were compared to our recent static light scattering measurements in the same system. In general, good agreement was found for all four parameters. However, monomer number and size from light scattering have a considerable spread due to uncertainties in soot refractive index and a morphological parameter describing the proportionality between monomer number and radius of gyration. We conclude that current theories of fractal cluster scattering and absorption have no egregious errors, but a stringent test could not be made, and that light scattering and mechanical probing yield consistent results.

I. Introduction

With the development of the fractal concept for describing clusters of particles and the realization that random aggregation processes lead to fractal clusters,[1-3] our ability to describe and quantify the morphology of clusters so generated was significantly improved. This engendered the problem of how to experimentally determine cluster morphological parameters such as the radius of gyration, R_g, the fractal dimension, D_f, the number of monomers per aggregate, N, and the monomer radius (assumed spherical), a. This is a problem for both visual inspection via transmission electron microscopy and more so for light scattering measurements. In fact use of light scattering required theoretical work to determine how a fractal cluster scatters and absorbs light.[4-8]

Recent work has used in situ light scattering to determine size and structure of soot particles in flames with the fractal concept[9-15] and has relied upon these theories and the assumptions made in them to analyze the data. Our work[9-12] has used both optical structure factor measurements (scattered intensity as a function of scattering angle) and scattering/extinction measurements. We have shown how R_g and D_f can be measured, and if the two methods are combined, N and a can be determined as well.[11] It would be useful and important, however, to be able to make direct comparisons of these optical measurements with soot particles physically sampled from the flame. This would serve as a test of the theory for the optics of fractal clusters. It would also substantiate our ability to make in situ optical measurements. Although soot sampling with an external probe is notoriously intrusive, Dobbins and Megaridis[16] have developed a thermophoretic sampling method which is fast, unbiased on size, and as unperturbative as possible. Soot collected from a flame by this method has been examined by electron microscopy, and in some cases, comparisons with light scattering results been made.[9,17,18] No efforts, however, have been attempted to make a full, comprehensive comparison of the above mentioned soot morphology parameters determined by light scattering and electron microscopy.

The purpose of this paper is to make such a comparison. We have collected soot from the same premixed methane/oxygen flames used in our previous light scattering studies.[10-12] TEM micrographs of the soot were digitized by an optical scanner and these digitized images were stored in a computer. The images were computer processed to remove unwanted background darkness levels. The images were used in two different formats, a 16-shade format, which preserved three-dimensional information for the clusters despite their projection onto a two-dimensional plane by the electron microscope, and a two-shade format in which the cluster was uniformly dark and the background uniformly bright. The two formats have allowed us to accurately assess the effects of the three- to two-dimensional projection process, inherent in electron microscopy, on the measured size and morphological parameters. The TEM measurements of R_g, D_f, N (hence mean size, see below), and a were then compared to previous light scattering measurements[11] from the same flame.

II. Experimental Method

Our experimental apparatus was the same as that used previously.[10-12] Our flame was supported on a cooled porous frit burner obtained from McKenna Products. The premixed gases passed through a 6 cm diameter porous frit. This frit was surrounded by an annular sheath region 0.5 cm wide through

® Abstract published in *Advance ACS Abstracts*, September 15, 1993.

(1) Forrest, S. R.; Witten, T. A. *J. Phys. A: Gen. Phys.* 1979, 12, L109.
(2) Family, F.; Landau, D. P., Eds. *Kinetics of Aggregation and Gelation*; North Holland: Amsterdam, 1984.
(3) Stanley, H. E., Ostrowsky, N., Eds. *On Growth and Form*; Nijhoff: Boston, MA, 1986.
(4) Berry, M. V.; Percival, I. C. *Opt. Acta* 1986, 33, 577.
(5) Freltoft, T.; Kjems, J. K.; Sinha, S. K. *Phys. Rev. B: Condens. Matter* 1986, 33, 269.
(6) Teixeira, J. In ref 3.
(7) Mountain, R. D.; Mullholland, G. W. *Langmuir* 1988, 4, 1321.
(8) Nelson, J. *J. Mod. Opt.* 1989, 36, 1031.
(9) Zhang, H. X.; Sorensen, C. M.; Ramer, E. R.; Olivier, B. J.; Merklin, J. F. *Langmuir* 1988, 4, 867.
(10) Gangopadhyay, S.; Elminyawi, I.; Sorensen, C. M. *Appl. Opt.* 1991, 25, 4859.
(11) Sorensen, C. M.; Cai, J.; Lu, N. *Appl. Opt.* 1992, 31, 6547.
(12) Sorensen, C. M.; Cai, J.; Lu, N. *Langmuir* 1992, 8, 2064.
(13) Hurd, A. J.; Flower, W. L. *J. Colloid Interface Sci.* 1988, 122, 178.
(14) Bonczyk, P. A.; Hall, R. J. *Langmuir* 1991, 7, 1274.
(15) Charalampopoulous, T. T.; Chang, H. *Combust. Flame* 1991, 87, 89.

(16) Dobbins, R. A.; Megaridis, C. M. *Langmuir* 1987, 3, 254.
(17) Samson, R. J.; Mulholland, G. W.; Gentry, J. W. *Langmuir* 1987, 3, 273.
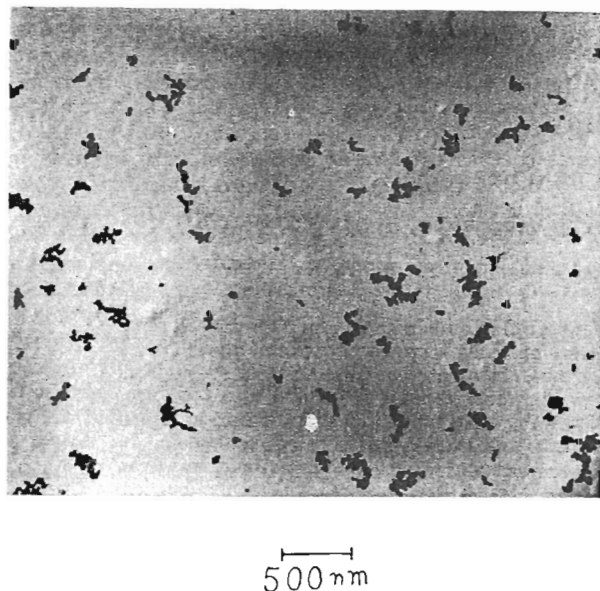(18) Megaridis, C. M.; Dobbins, R. A. *Combust. Sci. Technol.* 1990, 71, 95.

$\overline{500 \, nm}$

Figure 1. TEM micrograph of soot clusters collected at a height of 18 mm above the burner surface. Probe residence time was 15 ms.

which nitrogen was passed. A 15 cm diameter steel stagnation plate was placed 30 mm above the burner surface to stabilize the flame.

The gases used were methane and oxygen premixed before the burner. Their flows were controlled by critical orifices which we calibrated with a dry-test flowmeter. The cold gas velocity, uniform across the frit, of the mixture was 6 cm/s. The nitrogen sheath flow was also critical orifice controlled to a velocity of 5 cm/s. This arrangement yielded a quasi-one-dimensional flame with the only major variable being the height above the burner, h. The fuel to oxidizer ratio of these flames is described by the ratio of carbon atoms to oxygen atoms, C/O, in the gas mixture. We used C/O = 0.75, which was one of the two ratios we used for our light scattering measurements.[11] The C/O ratio for complete combustion to H_2O and CO_2 is 0.25.

We built a thermophoretic soot sampling device similar to that developed by Dobbins and Megaridis.[16] The metal collector probe residence time in the flame was monitored. The entrance and exit times, during which the probe traveled 5 cm, were ~5 ms. Formvar coated copper TEM grids were mounted onto the metal probe by epoxy glue.

The flatness of the flame, i.e. uniformity across a given diameter, was checked as described in one of our previous papers.[10] The flame was flat; hence a uniform sampling of soot particles could be obtained. The stagnation plate was cleaned of built up soot every time soot was to be collected. Soot samples were collected at heights of 12 and 18 mm above the burner surface. The probe and grids were inserted in the vertical plane for minimum effect on the flame flow, with residence times of 15, 50, and 100 ms. Then the grids were examined with a transmission electron microscope (TEM) and negatives of soot pictures were obtained at a magnification of 19 200. For pictures obtained with 50 and 100 ms residence times, the ratios of soot area to total picture area were 0.10 and 0.19, respectively, and cluster overlapping may have occurred. On the other hand for a 15-ms residence time, this ratio was 0.03; hence the chance of having overlapping clusters was quite low. Figure 1 shows a TEM micrograph obtained at h = 18 mm and a residence time of 15 ms. We used the pictures with a 15-ms residence time in our analysis. The final soot prints, enlarged by a factor of 2, were scanned into PCX format files in 16 shades of gray using a Niscan scanner. The picture resolution used was 0.2 mm per pixel. Considering the magnification of the picture, this resolution was equivalent to 5.2 nm per pixel, which was less than the size of a monomer in our case. A picture editor was used to carefully remove all unwanted darkness in the picture background not
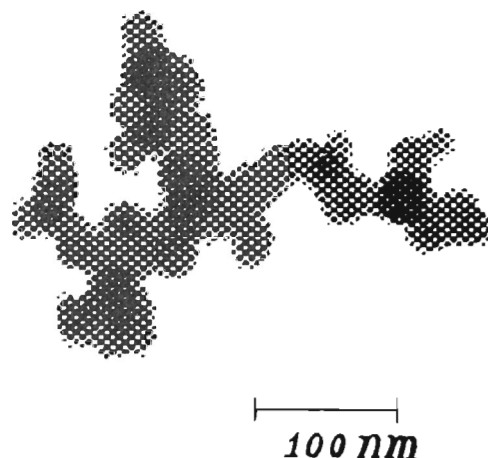

$\overline{100 \, nm}$

Figure 2. Example of computer digitized soot image in 16-shade format.

belonging to a cluster (including unoccupied areas within the cluster) in order to get a clean picture of the soot clusters; that is, all background was white and only sites occupied by the clusters were dark (15 levels of different shades). Figure 2 shows a large cluster after 16-shade digitizing and computer editing.

The soot clusters were sampled from the pictures in two different ways at each height. A large area was examined with ca. 200 clusters and the largest 20 clusters were chosen. We will call this set of clusters "Biggest" because it represents the biggest clusters in a given large area of the micrograph. A second sampling involved picking a smaller picture area and using all the clusters (there were 26 at each height) in the area. We will call this set of clusters "All".

III. Analysis

A major problem in the morphology analysis of TEM micrographs of soot clusters is that the images represent projections of the three-dimensional clusters onto a two-dimensional, x–y, plane.[18,19] Thus information regarding the third dimension may be lost. As described above, however, our soot cluster images are stored in the computer in a 16-shade format. These shades of darkness retain some, if not most, of the information of the third dimension. We need to determine if this format retains sufficient three-dimensional information for a viable analysis of our clusters.

A. Darkness. We define the total darkness of a cluster obtained from the 16-shade information as D_{16}. D_{16} can be calculated for a given cluster by summing all the individual darkness levels for all the pixels in the cluster

$$D_{16} = \sum_{x,y} D(x,y) \qquad (1)$$

This sum is over all the pixels designated uniquely by the ordered pairs (x,y). We contend that this is proportional to the total mass, hence the total number of monomers in the cluster, under the assumption that all the monomers have the same total darkness. This assumption is probably not exact, but even then D_{16} is proportional to a useful effective average number of monomers.

One may convert the 16-shade format into a 2-shade format by setting $D_2(x,y) = 1$ if $D(x,y) > 0$ and $D_2(x,y) = 0$ if $D(x,y) = 0$. Then one may define a 2-shade, or binary, total darkness as

$$D_2 = \sum_{x,y} D_2(x,y) \qquad (2)$$

Obviously, D_2 is proportional to the total projected area of the cluster.
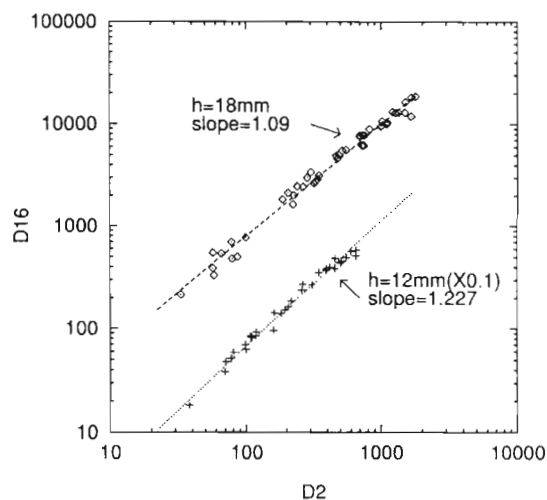
(19) Weitz, D. A.; Huang, J. S., In ref 2.

Figure 3. 16-shade versus 2-shade total darkness of the clusters.

We now check the self consistency of the definitions of D_2 and D_{16} and the contention that $D_{16} \propto N$, where N is the number of monomers in the cluster. To do this we plot D_{16} vs D_2 for all the clusters studied for both heights above the burner on a log–log graph in Figure 3. The linearity of these graphs implies the power law relationships

$$D_{16} \propto D_2^{1.23}, \quad h = 12 \text{ mm} \tag{3a}$$

$$D_{16} \propto D_2^{1.09}, \quad h = 18 \text{ mm} \tag{3b}$$

It has been found empirically that the total number of monomers in a soot cluster is related to the projected area by[18,20–22]

$$N = (A_c/A_m)^\alpha \tag{4}$$

where A_c is the total area of the cluster and A_m is the average monomer area, and where $\alpha = 1.09$ for $5 < N < 505$. For $h = 18$ mm, eq 3b is in good agreement with this result to imply $D_{16} \propto N$ and $D_2 \propto A$ as we contend. Our TEM results yield average values of the mean size in the range 10 to 22 monomers per cluster (s_1 and s_2, see below) for this height. For $h = 12$ mm, eq 3a suggests $\alpha = 1.23$, larger than expected from the earlier work.[18,20–22] However, TEM analysis yields a mean size in the range 6 to 11 (s_1 and s_2) for this height which may be too small for the empirical result (4) to hold. To support this one may consider the $N \to 1$ limit, i.e., a solid sphere. Then we expect $D_2 \propto R^2$, yet $D_{16} \propto R^3$ where R is the sphere radius. This yields $D_{16} \propto D_2^{1.5}$; i.e., $\alpha = 1.5$. Thus we view the result of eq 3a as giving a value of α that has left 1.09 and is approaching the limit 1.5 because the N value at this height is small.

B. Radius of Gyration. We continue our development of the meaning of D_2 and D_{16} and the consequences of 2-shade and 16-shade analysis by considering the cluster radius of gyration, R_g. The radius of gyration may be calculated in either the 2- or 16-shade format as

$$R_{g,2}^2 = D_2^{-1} \sum_{x,y} D_2(x,y)(\vec{r}(x,y) - \vec{r}_{cm,2})^2 \tag{5a}$$

or

---

(20) Samson, R. J.; Mulholland, G. W.; Gentry, J. W. *Langmuir* 1987, 3, 272.

(21) Medalia, A. I.; Heckman, F. A. *J. Colloid Interface Sci.* 1967, 24, 393; 1971, 36, 173.

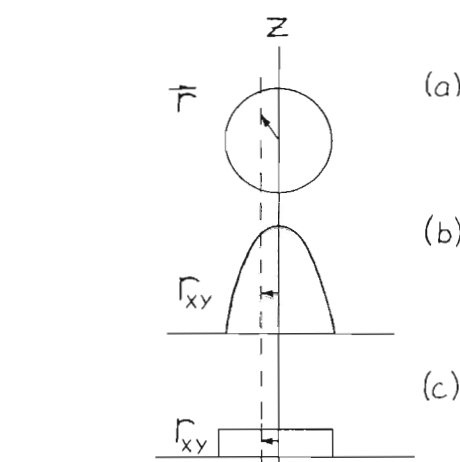(22) Koylu, U. O.; Faeth, G. M. *Combust. Flame* 1992, 89, 140.

Figure 4. Schematic of how a spherically symmetric cluster (a) can be projected onto a two-dimensional, x–y plane either preserving total mass information (b) or not (c).

$$R_{g,16}^2 = D_{16}^{-1} \sum_{x,y} D(x,y) (\vec{r}(x,y) - \vec{r}_{cm,16})^2 \tag{5b}$$

In eqs 5 $\vec{r}_{cm}$ is the position of the cluster center of mass found by

$$\vec{r}_{cm,2} = D_2^{-1} \sum_{x,y} D_2(x,y)\vec{r}(x,y) \tag{6a}$$

or

$$\vec{r}_{cm,16} = D_{16}^{-1} \sum_{x,y} D(x,y)\vec{r}(x,y) \tag{6b}$$

One can show in general that the projected R_g are less than the real, three-dimensional R_g. To see this, consider Figure 4 which represents a spherical cluster being projected onto two-dimensions. The radius of gyration is a root mean square (rms) radius relative to the center. An arbitrary vector $\vec{r}$ (Figure 4a) when projected can only become a shorter vector r_{xy} (Figure 4b,c). Hence the rms value must become smaller when total mass information is retained as in Figure 4b.

This argument can be quantified if we consider a spherically symmetric sphere with density given by

$$\rho(r) = \rho_o \, r^{D_f-d}, \quad r \le R \tag{7a}$$

$$= 0, \quad r \ge R \tag{7b}$$

Here $d = 3$ is the spatial dimension. This is an average density for a cluster of fractal dimension D_f. The density diverges at $r = 0$, but this represents no problem in our analysis. The radius of gyration of this sphere is

$$R_g^2 = \frac{D_f}{D_f + 2} R^2 \tag{8}$$

As an example consider a solid sphere with $D_f = 3$. Then eq 8 yields $R_g^2 = 0.6R^2$. A projection which retains total mass information, Figure 4b, has $R_g^2 = 0.4R^2$, a value equivalent to the radius of gyration about the z-axis through the three-dimensional sphere's center. We view this projection as approximated by the 16-shade format. Finally, projection to a 2-shade format yields a disk with $R_g^2 = 0.5R^2$ (eq 8 with $D_f = 2$). Thus we expect $R_g > R_{g,2} > R_{g,16}$.

Our data support this argument. Figure 5 shows $R_{g,2}/R_{g,16}$ versus $R_{g,2}$ for all our clusters at both heights. One sees $R_{g,2} > R_{g,16}$ as predicted. Equality is approached for large clusters because $D_f \simeq 1.75$, far less than $D_f = 3$ and
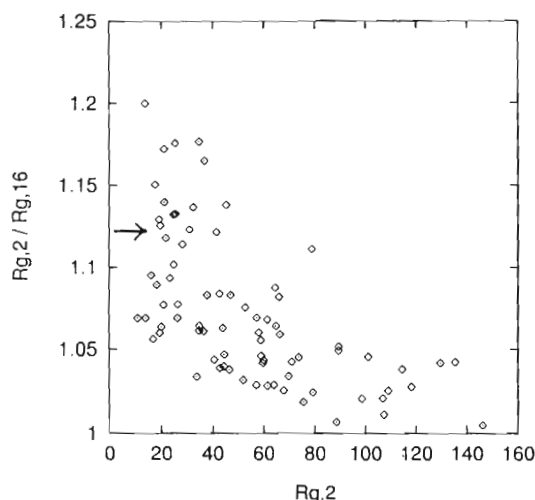
Figure 5. Ratio of the radius of gyration calculated in the 2-shade format to that from the 16-shade format, $R_{g,2}/R_{g,16}$, versus $R_{g,2}$. The arrow at $R_{g,2}/R_{g,16} = 1.12$ indicates the theoretical value for a dense, $D_f = 3$ sphere.

Table I. Radii of Gyration Determined by Various Means

	radius of gyration, R_g (nm)			
h, mm	all	all-corrected	biggest	light scattering
12	56	73	65	67
18	85	110	113	115

most importantly less than 2, the dimensionality onto which they are projected. Thus we expect these large, open clusters to look the same in either format. The small cluster limit in Figure 5 can be understood by realizing that this limit is the single monomer limit, i.e., a dense, $D_f = 3$ sphere. Then from the above numerical values we expect $R_{g,2} = 5^{1/2}/2R_{g,16} = 1.12R_{g,16}$. This point is marked in Figure 5 and one sees the small $R_{g,2}$ data cluster around this predicted limit.

Samson et al.[20] argued that occultation of monomers by other monomers during the projection process would affect the measured radius of gyration. They argued that since occultation was more probable near the cluster's center, the measured R_g would be ~10% *larger* than the true R_g. They failed, however, to account for the projectional shortening of the position vectors, which we have seen tends to make the measured R_g too *small*. We will show that both these effects tend to cancel each other for the two-shade projection.

Both effects, occultation and projectional shortening, can be modeled by considering the projection in Figure 4c, i.e., to a binary, two-shade disk. We again consider the projection of a sphere with a spherically symmetric density given by eqs 7. For $D_f \geq 2$ a two-shade, non-mass-conserving projection of the sphere will yield a uniform density disk (Figure 4c) with radius of gyration

$$R_{g,2}^2 = \frac{1}{2}R^2 \qquad (9)$$

Comparison of eqs 8 and 9 yields

$$R_g = \left(\frac{2D_f}{D_f + 2}\right)^{1/2} R_{g,2} \qquad (10)$$

Equation 10 implies $R_{g,2}$ is in error by at most 9.5% (too small) even at $D_f = 3$, i.e., a solid sphere. This is better than the error if no occultation occurs as in the mass preserving, Figure 4a to 4b projection, which for $D_f = 3$ yields a measured R_g 18% too small. Comparison of these numbers shows inclusion of occultation causes the measured R_g to increase by ~9% in agreement with the Samson et al. argument.

It is noteworthy that our model shows that $R_{g,2}$ is exact at $D_f = 2$, a value near the fractal dimension of soot. We argue that eq 10 does not hold for $D_f < 2$ because projection

of such a three-dimension fractal object into two dimensions cannot uniformly fill the two-dimensional plane contrary to our assumption leading to eq 9. Even if it did, the error in $R_{g,2}$ for a soot-like $D_f = 1.75$ is only 3.5% (too big). Thus given the proximity of the soot cluster D_f to 2.0, we conclude $R_{g,2} = R_g$ to better than a few percent.

In summary, from the consistency of the above considerations, we shall use with confidence the relations

$$R_{g,2} = R_g \qquad (11a)$$

$$D_2 \propto \text{cluster projected area} \qquad (11b)$$

$$D_{16} \propto \text{cluster monomer number} \qquad (11c)$$

III. Results

A. Radius of Gyration. The two-shade radius of gyration was calculated for each cluster in both data sets "All" and "Biggest". To compare to the light scattering measurements of R_g, these clusters must be averaged in the same way, as light scattering averages the clusters during a measurement. Since the small angle light scattering intensity is proportional to the cluster monomer number squared, the light scattering R_g is related to the moments of the size distribution by[11]

$$R_g^2 = a^2 k_0^{-2/D_f} M_{2+2/D_f} M_2 \qquad (12)$$

where a is the monomer radius and k_0 is defined in $N = k_0(R_g/a)^{D_f}$, and

$$M_i = \int_0^\infty N^i \, n(N) \, dN \qquad (13)$$

Equation 13 defines the ith moment of the size distribution $n(N)$. Equations 11a, 11c, 12, and 13 imply the average that must be made for our TEM clusters is

$$\langle R_g^2 \rangle = \sum_i D_{16,i}^2 R_{g,2,i}^2 / \sum_i D_{16,i}^2 \qquad (14)$$

Here the sum is over all members in the data set. Table I lists the results of these averages along with the light scattering results.

Comparisons of light scattering R_g values to the R_g values obtained from the "Biggest" data set at each height are quite good. We found that as we began to include the next smallest clusters of the remaining ~180 clusters on the picture from which these data sets were obtained, the average changed very little. In fact, assuming the remaining 180 clusters were all monomers and including these in the average of eq 14 changed the average R_g by only 1%. This can be understood as due to the weighting via $D_{16}^2 \propto N^2$ of the distribution of cluster sizes when the average is calculated. Light scattering sees only the large tail of the distribution. Inclusion of the remaining clusters on the picture would not significantly change the average value reported in Table I.

Average R_g values obtained from the "All" data set are seen to be 20–30% smaller than the light scattering values. We believe this is due to the smallness of our sample. A small sample will not include the rare large clusters which, by eq 14, dominate the average.

We can estimate the error a finite sample makes for the average R_g and thereby calculate a correction factor. We recall that the average R_g is related to the moments of the

size distribution through eq 12. Due to the limited sampling, the moments of the distribution should be modified for TEM measurements as

$$M_i' = \int_0^{N_{max}} N^i\, n(N)\, dN \qquad (15)$$

Suppose we used C clusters in our TEM measurements. The probability for chosing at random the largest of these clusters is $1/C$; thus we will assume that $1/C$ is also the total probability for $N > N_{max}$, then

$$1 - 1/C = \frac{\int_0^{N_{max}} n(N)\, dN}{\int_0^{\infty} n(N)\, dN} \qquad (16)$$

We now assume a scaling size distribution of the form[23,24]

$$n(N) = M_1 s_1^{-2} \phi(N/s_1) = M_1 s_1^{-2} \phi(x) \qquad (17a)$$

$$\phi(x) = e^{-x} \qquad (17b)$$

and

$$s_1 = M_1/M_0 \qquad (17c)$$

Then eq 16 yields

$$1 - 1/C = 1 - e^{-x_{max}} \qquad (18)$$

where $x_{max} = N_{max}/s_1$ and $x_{max} = 3.26$ if $C = 26$. For $D_f = 1.7$, which is a reasonable value for our soot clusters, we find

$$R_{g,TEM}^2 \sim \frac{\int_0^{3.26} x^{3.18} n(x)\, dx}{\int_0^{3.26} x^2 n(x)\, dx} = 2.24 \qquad (19)$$

or $R_{g,TEM} \sim 1.497$, while $R_{g,LS} \sim 1.94$ for the same distribution and D_f but with moments calculated with infinite upper limits. Therefore

$$\frac{R_{g,TEM}}{R_{g,LS}} = \frac{1.497}{1.94} = 0.77 \qquad (20)$$

This correction factor is used in Table I to generate corrected values of R_g for the "All" data. Now good agreement is found between these corrected values and the light scattering values.

In conclusion, both data sets are shown to yield good agreement between R_g values determined from TEM sampling and light scattering.

B. The Fractal Dimension. We have used three different methods to determine the fractal dimension D_f of our clusters obtained from the TEM study: (1) the method of successive squares; (2) the density correlation function; (3) comparison of R_g vs N for an ensemble of clusters. The first two methods look at and determine the fractal dimension for individual clusters. The third method considers the whole ensemble of clusters in the data set.

B.1. Successive Squares. In this method squares of side length s are computer drawn on the cluster centered on the cluster center of mass. The total darkness D is calculated for the area inside successive squares of increasing side length. If fractal, one expects $D \propto N \propto s^{D_f}$. This method will work best for large clusters such that the monomer size is small compared to the possible side lengths. Thus we applied this method to the four largest clusters in our combined data sets. The total darkness was calculated with both 2- and 16-shade formats for
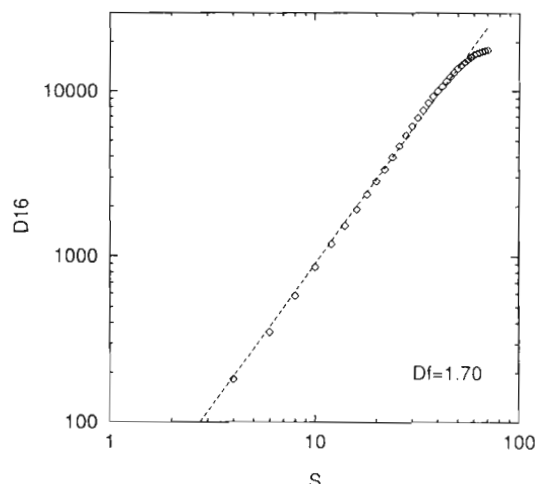
(23) van Dongen, P. G.; Ernst, M. H. *Phys. Rev. Lett.* **1985**, *54*, 1396.
(24) Mulholland, G. W.; Samson, R. J.; Mountain, R. D.; Ernst, M. H. *Energy Fuels* **1988**, *2*, 481.

Figure 6. 16-shade darkness within a box of side length s versus s for one of our larger soot clusters.

Table II. Fractal Dimension, D_f, Determined by Various Methods

method	D_f
successive squares, 2-shade	1.70 ± 0.07
successive squars, 16-shade	1.71 ± 0.10
correlation function, 2-shade	1.57 ± 0.08
correlation function, 16-shade	1.57 ± 0.08
ensemble of clusters (D_{16} vs $R_{g,2}$) $h = 12$ mm	1.93 ± 0.08
$h = 18$ mm	1.72 ± 0.07
light scattering	1.79 ± 0.10

comparison. A plot of D_{16} versus s for one of our clusters is given in Figure 6.

Table II gives the results for the successive squares methods. Small variation from cluster to cluster was seen and the average values given in Table II for both 2- and 16-shade darkness levels are essentially the same at $D_f = 1.7$. At first this is surprising given the results of Figure 3 that show $D_{16} \propto D_2^\alpha$, $\alpha > 1$. However, we picked our four largest clusters and for $D_f < 2$ one expects $\alpha \to 1.0$ as the cluster size becomes large,[25] also seen in Figure 3.

B.2. Pair Correlation Method. The density correlation function $c(r)$ is expected to scale as r^{D_f-d} for $R < R_g$. The Euclidean dimension d is two for our TEM analysis because the clusters were projected into two dimensions. We used an algorithm similar to that used by Samson et al.[20] We tested the algorithm using a uniform disk. Comparison of the density correlation function calculated by the algorithm and by analytical solution showed excellent agreement. We then calculated the density correlation function for the same four largest clusters used in the successive squares analysis. Once again either 2- or 16-shade darkness representations were used to calculate $c(r)$. By plotting $c(r)$ vs r on a log-log scale, the linear region gave slopes of $D_f - 2$ from which D_f was obtained. An example of such a plot is given in Figure 7. The values of D_f found by this method are given in Table II.

As for the successive squares method, some small cluster-to-cluster variation in D_f was seen, but the average values for either the 2- or 16-shade representations are equal at $D_f = 1.57$. Hence it seems once again that large clusters are little affected by the projection into two-dimensions. The value $D_f = 1.57$ is 8% lower than $D_f = 1.7$ obtained from successive squares. This difference is about the experimental error and so is marginally significant. This

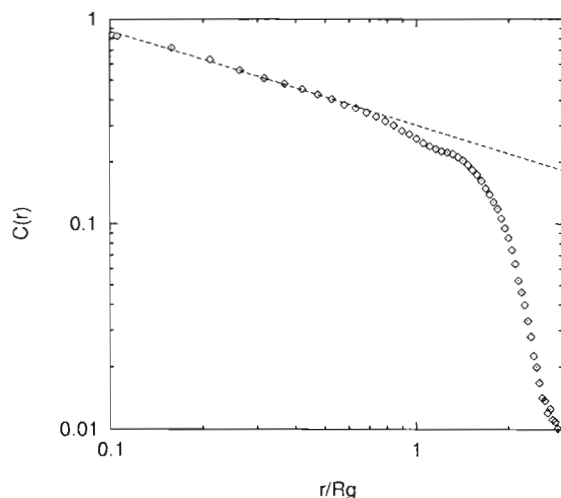(25) Meakin, P. *J. Colloid Interface Sci.* **1984**, *102*, 491.

Figure 7. Density correlation function for one of our larger soot clusters. Dashed line is the fit line to $c(r) \sim r^{D_f} r^{-2}$ to the first 13 points.
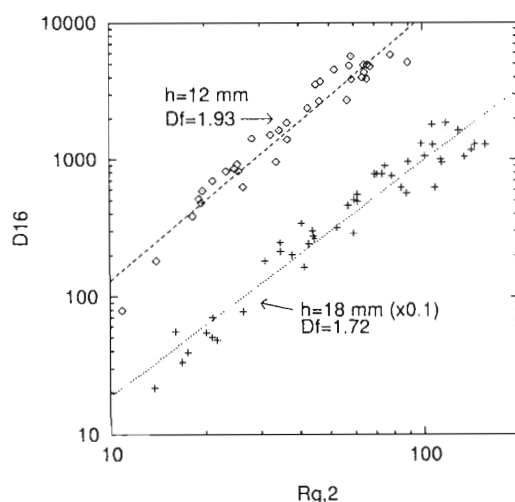

Figure 8. Total cluster 16-shade darkness versus 2-shade cluster radius of gyration for all the clusters in each data set ("All" and "Biggest") of each height h above the burner. Dashed lines are linear fits to yield the fractal dimension D_f.

is similar to the result of Samson et al.[20] who found values of D_f as much as 0.15 too low when determined from $c(r)$.

B.3. Ensemble of Clusters. The advantage of this method is that it uses all the clusters involved in the sample. The fractal dimension is found from the fact that $N \propto R_g{}^{D_f}$, hence from eq 11 we expect $D_{16} \propto R_{g,2}{}^{D_f}$. Plots of D_{16} vs $R_{g,2}$ on logarithmic scales for all the data at both heights are given in Figure 8. Good linearity is seen to imply the fractal nature and the slopes yield the fractal dimensions, which are tabulated in Table II.

For $h = 18$ mm, $D_f = 1.72$ which is in good agreement with the successive squares method and the values obtained from light scattering. At $h = 12$ mm, $D_f = 1.93$, which is slightly outside of experimental error high compared to other values. Recall, however, that at this height the clusters are small with only several monomers per cluster. Hence they are nearer the dense limit ($D_f = 3$) than at $h = 18$ mm. This fact was also seen in Figures 3 and 5.

In summary, fractal dimensions obtained from various analyses of the TEM micrographs of the clusters are in good agreement with the light scattering measurements.

C. Monomers per Cluster. Visual examination of

the cluster micrographs for direct counting of the monomers per cluster proved to be fraught with uncertainty. Often we found ourselves estimating monomer number in a given part of a cluster from the effective area of that segment. In fact, such a procedure has been quantified and used to determine monomer number via eq 4.

From eq 11c it would seem a more reasonable way to obtain N is by a ratio of D_{16} to the darkness of an average monomer. We found this latter quantity harder to quantify than either A_c and A_m and thus the uncertainty in the N value was larger than if we used eq 4.

We used eq 4 to determine N for our clusters in the "All" data set. For A_c the value of D_2 was used (eq 11b). For the monomer area the total darkness of ten different positively identified monomers was measured and averaged at each height. These averages had a standard deviation of 16%. These two darknesses, cluster and monomer, were then ratioed and raised to the α power where $\alpha = 1.23$ and 1.09 for $h = 12$ and 18 mm, respectively, in accord with our empirical results in Figure 3.

Before comparison to our light scattering results, we must contend with the assumptions that were involved in our light scattering work to determine the number of clusters per aggregate.[11] We assumed monodispersity in monomer size, which appears reasonable from our TEM work and which we continue to use without good knowledge of its consequences. We made an initial assumption that the clusters were monodisperse in N. Hence conversion to mean size values must be made using an appropriate size distribution. We assumed a value of $k_0 = 1.56$, which was calculated from the correct $N \rightarrow 1$ limit and was in reasonable accord with simulations.[7] And we assumed the soot refractive index was $m = 1.56 - 0.56i$;[26] hence $E/F = 1.22$ where $E = -\text{Imag}[(m^2 - 1)/(m^2 + 2)]$ and $F = |(m^2 - 1)/(m^2 + 2)|^2$.

We address first the assumption of cluster monodispersity. In our previous work we described how the value of N determined from our light scattering measurements under the assumption of cluster monodispersity could be converted into a mean size (eq 42 of ref 11) given by

$$s_i = M_i/M_{i-1} \qquad (21)$$

for $i = 1$. Note this definition has units of N, depends linearly on N, and increasingly tends to weight the large N part of the size distribution as i increases. The scaling distribution given in eq 17 yields $s_2 = 2s_1$ and $s_3 = 3s_1$.

N was determined by comparing R_g values to R_{SE}, the scattering/extinction radius

$$R_{SE} = k_0{}^{1/D_f} N^{1/3 - 1/D_f} R_g \qquad (22)$$

The scattering/extinction radius is defined in ref 11 and is a volume equivalent sphere radius. The largest errors come from our uncertainty in R_{SE} and k_0. R_{SE} is uncertain because the value of the soot refractive index m is not exactly known and related to m via $R_{SE} \sim (E/F)^{1/3}$. From (22) one finds

$$s_i \sim N \sim (E/F)^{-D_f/(3-D_f)} k_0{}^{3/(3-D_f)} \qquad (23)$$

In our light scattering analysis we used a value of $E/F = 1.22$. Other values of m in the literature[27] lead to smaller values of E/F down to 0.65. Since $D_f \simeq 1.75$, eq 23 shows that this corresponds to a possible range in N and hence the s_i values of a factor of 2.4.

(26) Dalzell, W. H.; Sarofim, A. F. *J. Heat Transfer* **1969**, *91*, 100.
(27) Vaglieco, B. M.; Beretta, F.; D'Alessio, A. *Combust. Flame* **1990**, *79*, 259.

Table III. Mean Number of Monomers Per Cluster

h, mm	TEM	$E/F = 1.22$ $k_0 = 1.56$	$E/F = 1.22$ $k_0 = 1.1$	$E/F = 0.65$ $k_0 = 1.56$	$E/F = 0.65$ $k_0 = 1.1$
12	$s_1 = 6$	8	4	20	9
	$s_2 = 11$	17	7	40	17
	$s_3 = 15$	25	11	60	26
18	$s_1 = 10$	17	7	42	18
	$s_2 = 22$	35	15	84	37
	$s_3 = 31$	53	23	127	55

Table IV. Monomer Size (nm) Determined by Various Means

h, mm	TEM	$E/F = 1.22$ $k_0 = 1.56$	$E/F = 1.22$ $k_0 = 1.1$	$E/F = 0.65$ $k_0 = 1.56$	$E/F = 0.65$ $k_0 = 1.1$
12	12	13	17	8	10
18	15	14	18	8	11

The constant k_0 was evaluated based on the proper $N \rightarrow 1$ limit for a fractal cluster. We now know that better values of k_0 can be obtained by considering other limits, e.g., dimers, trimers, etc.[28] We find $k_0 = 1.56$ is an upper bound and $k_0 = 1.1$ represents a reasonable lower bound to the possible range of k_0 (the best value may be $k_0 = 1.3$). By eq 23 with $D_f = 1.75$ this corresponds to N and hence s_i ranging by a factor of 2.3.

Thus we see N and consequently s_i are susceptible to large error due to the current deficiencies in our knowledge of cluster refractive index and morphology. We have included these possible extremes of range for E/F and k_0 in Table III. One sees a large variation with our original analysis near the center of the variation range.

The TEM mean sizes were calculated from the ensemble of cluster sizes for the "All" data and averaged according to eq 21 which yields

$$s_1 = \sum_i N_i / \sum_i 1 \tag{24a}$$

$$s_2 = \sum_i N_i^2 / \sum_i N_i \tag{24b}$$

$$s_3 = \sum_i N_i^3 / \sum_i N_i^2 \tag{24c}$$

where N_i is the number of monomers in the ith cluster. These values are also listed in Table III. Within a large range, the comparison between light scattering and TEM is good, although one might argue it would be hard to miss. It is important to note, however, that the TEM mean sizes fit well to a ratio of 1:2:3 as expected from the size distribution of eq 17, thus supporting our use of this distribution.

D. Monomer Size. The diameters of ten monomers at each height above burner were measured directly with a magnifier and averages taken. The light scattering measurement assumes monodispersity in monomer radius a; hence no special considerations for averaging need to be made. Once again, however, light scattering compares R_{SE} and R_g, assuming knowledge of E/F and k_0, to determine a. From our previous work and following logic similar to that which led to eq 23, one can show

$$a \sim (E/F)^{1/(3-D_f)} k_0^{1/(D_f-3)} \tag{25}$$

Table IV compares the monomer radius for TEM and light scattering. As for the size comparison, we calculate a for the extremes of the ranges $1.22 \geq E/F \geq 0.65$ and $1.56 \geq k_0 \geq 1.1$ and include them in Table IV.

Once again given the broad range in light scattering values, the comparison is good. Note that a does not range

as widely as size; it is not as strongly dependent on E/F and k_0. Furthermore, note fairly good agreement of TEM values with the center of the a range.

IV. Discussion and Conclusions

The radius of gyration and fractal dimension comparisons between light scattering and TEM were quite good. This is not surprising given the fact that both measurements have been well exercised in the past. The light scattering R_g measurement is based on the fundamental way in which radiation scatters from any particle, fractal or not,[29] and has seen extensive application, especially in biophysics.[30] Since the ascendancy of the fractal concept, numerous studies have appeared[2,3] to measure the fractal dimension of clusters using either scattering or TEM examination. Most of these studies have yielded the same D_f, to imply a direct comparison, such as ours, would be successful.

Monomers per cluster and monomer radius are more directly related to the first-order theories of scattering and absorption of fractal clusters.[4-7] Under the assumption of no intracluster scattering, these theories predict scattering and absorption to be proportional to $N^2 \sigma_{scat}^m$ and $N\sigma_{abs}^m$, respectively, where σ_{scat}^m is the monomer scattering cross section and σ_{abs}^m is the monomer absorption cross section. It is this assumption and these results that are tested when values of N and a are compared between the two methods.

Our comparisons, and hence our attempt to test these theories, are hampered by uncertainties in index of refraction, through E/F, and the cluster's morphology, through k_0. Within these large uncertainties the comparisons are good; hence the theories are substantiated. We can certainly claim no egregious deficiencies lie in the theory. On the other hand attempts to go beyond the first-order theories[8,31] have indicated that if modifications are to be made they may lie at the 10% level, which is not discernible in the work presented here. Furthermore it is expected that these modifications become more important in large clusters and our clusters are relatively small. Thus a stringent test has not been made here.

With further study of the morphology of fractal clusters, the uncertainly in k_0 can be trimmed down. We are currently actively pursuing this problem. The index of refraction, however, stands, as it long has, as a major uncertainty which may continue to plague future comparison tests with soot aggregates. Perhaps use of other, well-characterized materials would provide a better system for future work concerning the theory of fractal scattering and absorption. And, to turn night into day, perhaps the sensitivity of the results to E/F may eventually allow an accurate measurement of this quantity using light scattering and TEM comparisons.

We also remark that from the light scatter's point of view, we have tested the efficacy of the mechanical probing and TEM analysis. Perhaps, best said, light scattering and mechanical probing yield consistent results regarding cluster size and morphology.

(28) Unpublished work from this laboratory.

(29) For example see Glatter, O.; Kratky, O. *Small Angle X-Ray Scattering*; Academic: New York, 1982.
(30) Zimm, B. H. *J. Chem. Phys.* **1948**, *16*, 1099.
(31) Fuller, K. A. Preprint submitted to *J. Opt. Soc. Am.*